In Vivo Fate of Avidin-Nucleic Acid Nanoassemblies as Multifunctional Diagnostic Tools

Paolo Bigini,[†,#] Sara Previdi,[†,#] Elisabetta Casarin,[‡] Davide Silvestri,[‡] Martina Bruna Violatto,[†] Sonia Facchin,[§] Leopoldo Sitia,[†] Antonio Rosato,[⊥,○] Gaia Zuccolotto,[○] Nicola Realdon,[‡] Fabio Fiordaliso,[∥] Mario Salmona,[†] and Margherita Morpurgo[‡,*]

[†]Department of Biochemistry and Molecular Pharmacology, IRCCS-Istituto di Ricerche Farmacologiche "Mario Negri", Via La Masa 19, 20156 Milan, Italy, [‡]Pharmaceutical and Pharmaceutical and Pharmacological Sciences, Universtà di Padova, via Marzolo, 5, 35131 Padova, Italy, [§]ANANAS nanotech, s.r.l., via Altinate 120, 35131 Padova, Italy, [⊥]Istituto Oncologico Veneto IOVIRCCS, Via Gattamelata 64, 35128 Padova, Italy, [○]Department of Surgery Oncology and Gastroenterology, University of Padova, Via Gattamelata 64, 35128 Padova, Italy, and [∥]Department of Cardiovascular Research, IRCCS-Istituto di Ricerche Farmacologiche "Mario Negri", Via La Masa 19, 20156 Milan, Italy. [#]These authors contributed equally.

ABSTRACT This study describes the formulation optimization and body-cell distribution and clearance in mice of a dually fluorescent biodegradable poly avidin nanoassembly based on the novel Avidin-Nucleic-Acid-Nano-ASsembly (ANANAS) platform as a potential advancement of classic avidin/biotin-based targeted delivery. The nanoformulation circulates freely in the bloodstream; it is slowly captured by filter organs; it is efficiently cleared within 24−48 h, and it is poorly immunogenic. The system displays more favorable properties than its parent monomeric avidin and it is a promising tool for diagnostic purposes for future translational aims, for which free circulation in the bloodstream, safety, multifunctionality and high composition definition are all necessary requirements. In addition, the assembly shows a time-dependent cell penetration capability, suggesting it may also function as a NP-dependent drug delivery tool. The ease of preparation together with the possibility to fine-tune the surface composition makes it also an ideal candidate to understand if and how nanoparticle composition affects its localization.

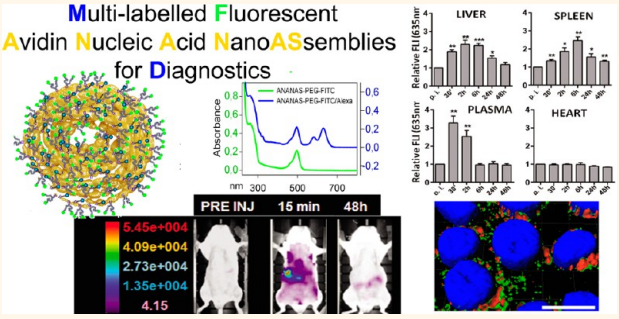

KEYWORDS: avidin nucleic acid nanoassemblies · poly avidin · fluorescence optical imaging · *in vivo* diagnostics · nanomedicine · multifunctional

In recent years, the active search for novel theranostic agents has led to the development of many kinds of nanoparticle-based technologies. Since the food and drug administration (FDA) approval of s uper paramagnetic iron-oxide NP in 1996, one of the main goals in clinical imaging has been to develop innovative tracers capable of providing longitudinal tracking in patients and improving diagnostics and prognostics by noninvasive procedures. This objective has also called up the attention of drug delivery system developers, with the ambitious goal to generate multimodal devices capable of combining improved pharmacokinetics and targeted localization with an efficient modality of anatomical tracking by means of imaging instruments. As a consequence, multifunctionality is becoming a key feature for the development of novel theranostic nanosystems.[1−9] The challenge in this area is related to the possibility to not only load onto the nanoparticle (NP) different bioactive/tracer functions, but also be able to tune and control their individual payload. In this way, it is possible to establish a quantitative correlation between composition and bioactivity in order to tune the final device properties according to specific needs.[10] Therefore, the availability of reproducible and convenient standardized preparation methods that permit fine-tuning of each individual component becomes an important add-on to favor clinical translation and meet industrial interest.

In this context, the Avidin-Nucleic-Acids-Nano-ASsembly (ANANAS) represents an innovative NP platform[11] characterized by easy tuning of formulation composition and

* Address correspondence to margherita.morpurgo@unipd.it.

Received for review May 27, 2013 and accepted December 5, 2013.

Published online December 05, 2013
10.1021/nn402669w

surface chemistry properties. The term "ANANAS" refers to a series "poly-avidin" NP formulations originating from the high affinity interaction of avidin with the nucleic acids.[12] These buffer soluble NPs are formed by a *Nature*-driven double self-assembly in which, initially, a nucleic acid molecule acts as a central element around which several avidins (1 each 14 base pairs) nucleate, leading to toroidal assemblies (diameter about 120 nm);[12] in a second self-assembly process, a defined amount of biotinylated poly(ethylene glycol) (PEG) is also added to permit buffer solubility and increase stability.[13] In the end, the ANANAS assembly is a 'polymerized' form of avidin, one of the most renown proteins used in biomedicine,[14−17] and can be considered as a powerful alternative to it in many of its applications. Importantly, the ANANAS assemblies are composed of soft biocompatible materials only and, as opposed to other poly avidins obtained by chemical cross-linking or nonspecific adsorption onto metal or polymer substrates,[18−27] they are characterized by high composition definition. In addition, avidin in the assembly maintains its full biotin (B) binding capacity[11] so that the system carries a precisely defined number of biotin binding sites (BBS), which are available for docking additional biotinylated functional moieties.

The ANANAS platform can be deployed into several formulation compositions depending on the length of the nucleating nucleic acid and the kind and amount of biotinylated functions linked to the surface.[13] For example, recently, several functionally active ANANAS formulations generated through a "one-pot" procedure have been compared in a model of *in vitro* immunodetection, showing differently improved performance with respect to 'monomeric' avidin (namely reducing to different extent the analyte limit of detection down to a maximum 500-fold).[11] On top of its most renown application as an *in vitro* diagnostics tool, the avidin (and its bacterial analogue steptavidin)/biotin system is also extensively investigated as a carrier for targeted radio-diagnostics and therapy.[17,28−32] However, the success of (strept)avidin based targeting approaches has been limited by both unfavorable proteins pharmacokinetics[28] and, especially in the case of streptavidin (StAv), high immunogenicity.[17,33−35] In the context of targeted delivery, fast clearance of the nontargeted carrier is needed to avoid high background or long-term exposure of nontarget compartments to the (toxic) carried drug. On the other hand, an excessively fast elimination is also detrimental because it impedes the efficient tracking necessary in diagnostics and the (slow) diffusion processes necessary to reach target tissues necessary in drug delivery applications. StAv exhibits high and prolonged (>96 h) permanence in many tissues due to a RGD-like motif within its 58−62 amino acid sequence,[28] while avidin, whose fate also depends on its surface charge and varies with its degree of biotinylation,[36,37] has lower organ retention than StAv, but it is cleared from the bloodstream too rapidly (within 10 min) .[28]

To improve the poor pharmacokinetics/immunogenic profile of avidin/streptavidin, several protein derivatives have been obtained throughout the years, which have been tested within many administration protocols, with some success.[17,28−32,38] In the case of avidin, improvement of plasma half-life and minimization of its interaction with the immune system were obtained through its covalent conjugation with poly(ethylene glycol) (PEG).[38,39] However, the covalent attachment of PEG leads to partial loss of the protein biotin binding ability,[40] thus reducing its activity. Presently, the issue of the (strept)avidin unfavorable pharmacokinetics upon *i.v.* administration is not yet fully solved so that the most current promising use of the avidin/biotin system in targeted radio-therapy involves the intraoperative local administration of an oxidized protein derivative.[29]

Another possibility to modify the biodistribution and clearance of proteins characterized by poor pharmacokinetics is to formulate them into NP preparations. The ANANAS assembly here investigated is indeed a novel form of PEG coated poly avidin nanoformulation, and therefore, it could represent an avidin-based delivery device alternative to the "monomeric" protein. In this work, we investigated the *in vivo* fate upon iv administration of an ANANAS formulation, which was made dually fluorescent by using two biotin-labeled fluorophores (fluoresceine and alexa^{633}). NP dual fluorescent labeling was performed to allow concurrently fine composition control and to enable *in vivo* biodistribution studies through noninvasive *in vivo* Fluorescence optical imaging tools. The fluoresceine tag, which was linked at the ω-end of the biotin-PEG derivative introduced for surface protection, was used to permit precise estimation of the number of polymer chains linked to the particle. It also complemented the *in vivo* and *ex vivo* biodistribution information, which was mainly obtained through the alexa^{633} fluorophore.

RESULTS AND DISCUSSION

Formulation Optimization. One of the unique properties of the ANANAS platform is that it allows fine tuning of its surface tethered biotinylated moieties, permitting high control of the assembly composition. This permits an infinite number of surface composition combinations, the selection of which is to be chosen beforehand or in parallel to any functional evaluation. In the specific context of this work, we carried out **preformulation** studies to optimize the NP composition on the basis of two main requirements: (a) maximal PEG surface protection to favor stealthiness and (b) efficient alexa^{633} payload to allow *in vivo* near-infrared (NIR) visualization. It is known[23,41,42] that the fate of a NP is influenced by its degree of PEG coating,

(4) Biotin-CONH(CH_2)$_6$-NH-CO-PEG_{5K}-NH-Fluoresceine

(6) Biotin-CONH(CH_2)$_6$-NH- (NH-PEG_{5K}-NH-Fluoresceine; HN-PEG_{5K}-NH-Fluoresceine)

(7) Biotin-CONH(CH_2)$_6$-NH-CO-$Alexa_{633}$

Figure 1. The biotin fluorophores synthesized for this work.

the higher, the better is for the particle ability to freely circulate in the bloodstream. In fact, the hydrophilic polymer layer shields the particle from the body defenses and favors its stealth properties.

The preformulation studies were meant to estimate the maximal load possible for a 5 kDa PEG (PEG_{5kDa}) molecule and to evaluate if the polymer shape affects this parameter. It was previously shown, using biotinylated proteins as bulky cargoes, that the ANANAS loading capability is dictated by steric limitation rather than the available BBS.[11] On the other hand, it has not been shown if a particle saturated with a large MW cargo is still able to accommodate small biotin derivatives that, in principle, could be able to diffuse through small openings of the surface covering layer. A further goal of the preformulation studies was therefore to test if particles already saturated with a dense PEG layer were still able to load lower molecular weight biotin derivatives.

To evaluate if the shape of the polymer has any effect on the particle loading ability, two ω-FITC labeled biotin PEG derivatives were synthesized, namely a linear (5 kDa) one, and a branched one in which two FITC-PEG_{5kDa} chains are linked at the two primary amines of a biotin−lysine conjugate (Compounds **4** and **6**, Figure 1, see also Supporting Information, Figure S-1).

A buffer stable 'core' formulation was prepared by using the branched fluorescent derivative (compound **6**) at 1:1 molar ratio with respect to avidin, according to what described by Pignatto.[13] The number of PEG_{5kDa} chains linked to the resulting particle surface was calculated to be about 430 (16% of the theoretically available BBS), based on the amount of FITC measured from the assemblies UV spectra recorded after gel permeation purification.

After purification and characterization, this formulation was further added of oversaturating amounts of either the linear or branched derivative. After this second addition, about 700 PEG_{5kDa} chains/NP (Figure 2B) were found, independently of the PEG derivative used, confirming that steric hindrance is more important that the number of available BBS. Taking into account the ANANAS surface area available (6000 nm^2)[11] and the foot-print of a PEG_{5kDa} chain in mushroom conformation (25−30 nm^2),[43] the 700 PEG chains obtained at maximal polymer load must be organized in a mixed

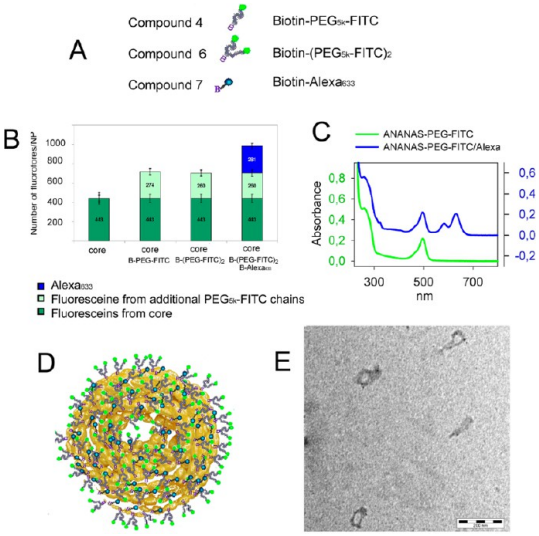

Figure 2. Schematic representation of the preformulation studies: (A) cartoon (not in scale) depicting the fluorescent biotinylated elements used for the preformulation studies; (B) summary of the loading capability of the ANANAS system with the fluorescent biotin derivatives; (C) cartoon depicting the PEG-FITC-ANANAS-alexa^{633} formulation selected for the *in vivo* studies; (D) UV spectra of the selected PEG-FITC-ANANAS NP before and after the addition of B−C_6-alexa^{633}; (E) electron microscopy images, size bar, 100 nm.

brush-mushroom conformation, which is ideal for minimizing undesired nonspecific interactions.[44−46] The formulation obtained with the "Y" shaped derivative (that contains one biotin every two PEG chains) is characterized by a higher number of free biotin binding sites (about 75% of total) and was therefore selected for further experiments. The ability of this formulation to accommodate additional smaller biotinylated compounds was verified. B−C_6-alexa^{633} (compound **7**, Figure 2 and Supporting Information) was added in molar excess, and after purification, 280 fluorophores were found to be stably linked. This formulation (PEG-FITC-ANANAS-alexa^{633}, Figure 2C,D), containing 700 PEG_{5kDa} chains deriving from the branched polymer derivative and 280 alexa^{633} residues (final 46% of BBS occupancy), having an average size (by DLS) of about 130 nm and an almost neutral surface charge (ζ-potential ≈ -5 mV (Table S-2 in Supporting Information)), was selected for the *in vivo* and *ex vivo* experiments.

Stability of the ANANAS Complex in Serum and Organ Extracts. Another peculiar property of the ANANAS formulation is that it is composed of soft biodegradable components only, and its assembly relies primarily on *Nature*-driven high affinity interactions. On one hand, these properties may be useful because the system is likely to be well tolerated after parenteral administration, on the other hand they make it potentially prone to biodegradation even in mild conditions, as for example, physiological buffers or body fluids. NP degradation, which would also impair *in vivo* data

analysis, could occur because of avidin disassembly from the core and/or detachment of the biotinylated elements (B-PEG-FITC and B−C_6-alexa^{633}) upon either loss of biotin binding capability or endogenous enzymatic biotinidase activity[47,48] on the biotin-linked moieties. The avidin/biotin interaction is governed by a 10^{-14}−10^{-15} M^{-1} dissociation constant, and since the affinity of avidin for free biotin is higher than for biotin-derivatives, detachment of the biotinylated moieties can be slowly reversed by the presence of endogenous biotin, or avidin denaturation. On the other hand, disassembly of the avidin-nucleic-acid core (avidin/DNA $K_d \approx 10^{-8}$−10^{-9} M^{-1}),[49] which is stabilized after its formation by a mild and reversible cross-linking, may be driven by multiple phenomena, including degradation of the avidin or DNA components and hydrolysis of the reversible stabilization chemistry, followed by DNA/avidin disassociation according to the equilibrium constants.

The robustness of the assembly to degradation in *in vivo*-simulating environments (namely plasma and metabolic organ homogenates) was therefore verified prior to *in vivo* analyses, in order to confirm that any signal later registered in animals was related to the original assembly and not to its degradation products. Stability tests (Figure 3) were carried out on the dually fluorescent NPs and on B−C_6-alexa^{633} when free in solution. More in detail, samples were incubated at 37 °C with liver or spleen homogenates;[50] plasma; or 10 mM phosphate, 150 mM NaCl, pH 7.4 (PBS) as a control, and their degradation was evaluated at different time points using two gel permeation chromatography tools, namely a G25 medium in a gravity column and Superose-6 (Superose) column on a FPLC apparatus. The first chromatography medium allows distinguishing between free or avidin-associated (NP-assembled or free in solution) low molecular weight fluorophores; it also allows distinguishing between B−C_6-alexa^{633} and its hydrolyzed alexa^{633}-COOH derivative (Figure S-8 in Supporting Information). The second medium allows differentiating between NP-bound avidin from its disassembled "monomeric" form.

B−C_6-alexa^{633}, when free in solution, was hydrolyzed into its COOH derivative, likely because of endogenous biotinidase activity, with the fastest kinetic in liver extract, followed by plasma and, finally, spleen extract (Figure 3A). However, when tethered to the nanoassembled avidin, its susceptibility to hydrolysis in plasma was dramatically reduced. As shown in Figure 3B, only organ homogenates were able to slowly detach the fluorophore from avidin (liver more efficiently than spleen), whereas incubation in plasma did not show any significant difference from PBS treatment. FPLC analysis was carried out at one time point only (15 h) (Figure 3C−E). Incubation in PBS alone lead to 30% reduction in NP content (peak at 7.6 mL), together with the formation of lower molecular weight NP

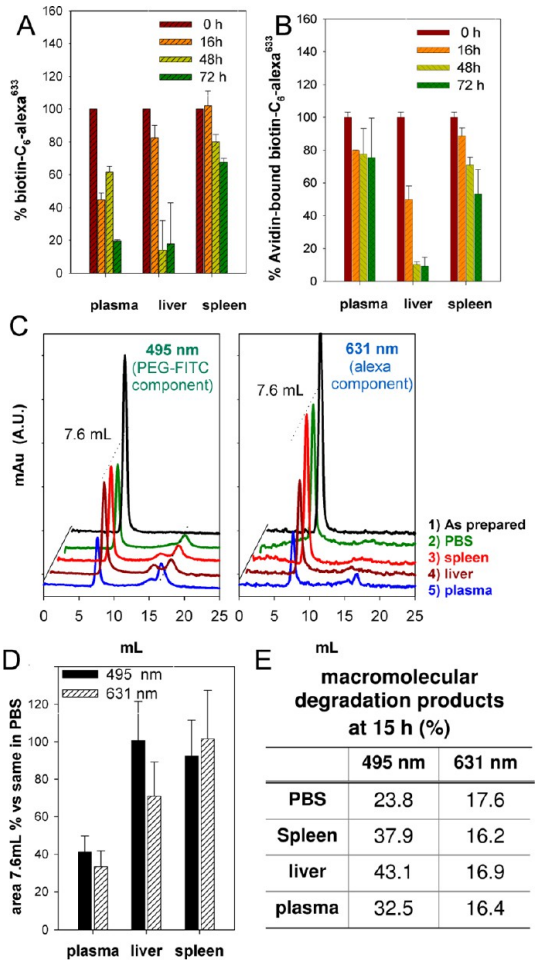

	495 nm	631 nm
PBS	23.8	17.6
Spleen	37.9	16.2
liver	43.1	16.9
plasma	32.5	16.4

Figure 3. Stability of B−C_6-alexa^{633} (A and B) and PEG-FITC-ANANAS-alexa^{633} (C−E) upon incubation at 37 °C in different physiological simulating environments. (A and B) Time-dependent residual (%) B−C_6-alexa^{633} after incubation, as such (A) or when linked to ANANAS (B) with organ homogenates. C) FPLC superose-6 gel permeation chromatograms registered at 495 and 631 nm of PEG-FITC-ANANAS-alexa^{633}, (1) as prepared, and after incubation at 37 °C for 15 h with (2) PBS, (3) spleen or (4) liver extracts and (5) plasma. (D) The area of the plasma or organ homogenates FPLC peak eluting at 7.6 mL, corresponding to the nanoassemblies, was normalized to that of the control sample incubated in PBS. (E) Area of the 495 and 631 nm absorbing components eluting between 14 and 17 mL, related to fluorescent NP degradation products, normalized to the as-prepared NP fluorophore content.

degradation products, whose retention volumes correspond to those of PEGylated avidin (14.9 mL) and biotin-(PEG-FITC)$_2$ (16.4 mL).

Instability in PBS is not surprising for a system like ANANAS, that relies for its assembly mostly on noncovalent high affinity interactions only. In fact, a 15 h treatment at 37 °C can also affect the stability of stable proteins like avidin, which consequently would either release some of its biotin linked moieties and/or detach from the core assembly. Liver and spleen incubation caused similar reduction in NP content as PBS, whereas incubation with plasma leads to 60−70% reduction in NPs as compared to PBS alone (Figure 3D). Since plasma

decrease was not accompanied with any increase in low molecular weight derivatives, this result can be explained only by the formation of large particle aggregates (still soluble), maybe secondary to opsonization by plasma proteins. These aggregates are undistinguishable from the original NPs using the larger mesh G25 chromatography medium (Figure 3B), but they are blocked by the superose column prefilter. Analysis of the NP degradation products eluting between 14 and 16 mL shows slightly faster degradation in the biological samples as compared to PBS. The NP component that is mostly susceptible to degradation is the one linked to the Biotin-(PEG-FITC)$_2$ moiety that showed a larger difference between PBS and homogenate treatment (Figure 3E). On the contrary, no detectable difference between PBS- and homogenate-treated samples was registered from the chromatograms registered at 631 nm. Since the NP peak maintains both FITC and alexa^{633} associated absorbance, we can conclude that any fluorescence associated signal *in vivo* is mostly related to NP-associated avidin and not to degradation products.

Immunogenicity. The response of the immune system is a fundamental parameter that needs to be taken into consideration when investigating any novel supramolecular delivery tool intended for parenteral administration. A strong immune reaction is not only risky for the patient, but also can promote the early sequestration of the delivered entity and reduce its efficacy. In the case of the ANANAS system, which is composed for most part of the exogenous protein avidin, an immunoresponse is indeed expected. However, it was also shown in experiments in humans that the immunoresponse induced by the monomeric avidin is not dangerous to the patients,[33] making it possible to envision its use also within the ANANAS supramolecular assembly.

The **immunogenicity** of the ANANAS formulation was therefore evaluated and compared to that of monomeric avidin as such or in the form of the complex with B-(PEG-FITC)$_2$ (compound **6**) (1:1 (mol/mol), avi:B-(PEG-FITC)$_2$) used for ANANAS assembly. Animals injected with monomeric avidin as such or complexed with biotin-(PEG-FITC)$_2$ raised antibodies specific for both antigen forms, with higher affinity for the non-PEGylated one (Figure 4). The avidin:B-(PEG-FITC)$_2$ complex led to the fastest and highest response, probably due to its longer body residence[39] (Figure S-9 in Supporting Information). The antibodies generated upon injection of this complex were also able to recognize the immobilized ANANAS. Interestingly, administration of the ANANAS formulation led to the lowest immune response. Low levels of antibodies against the two monomeric forms of avidin were raised after the third boost only, but these antisera failed to recognize the protein when within the ANANAS assembly.

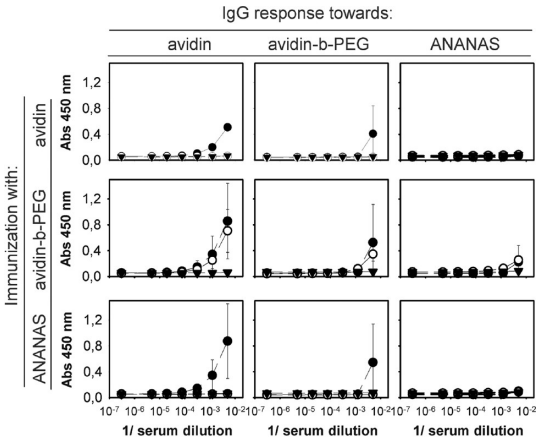

Figure 4. Results of the immunogenicity tests: anti-avidin, anti-avidin:biotin-(PEG-FITC)$_2$ and anti-PEG-FITC-ANANAS antibody titer in mouse sera harvested one week after one (▼), two (○) or three (●) s.c. administrations of each of the three samples diluted in PBS. Avidin, avidin:B-(PEG-FITC)$_2$ and PEG-FITC-ANANAS coated NUNC maxisorp 96-well microplates were generated by incubating each of the above reagents with microplates previously saturated with biotinylated BSA (see Supplemetary Information). After incubation with serial dilutions of the mouse sera, the relative level of all antigen-specific mouse IgGs was compared through the signal generated after anti-mouse-horseradish peroxidase (HRP) incubation and 10 min of TMB color development.

These results can only be explained by assuming that the avidin in the particles is highly shielded by the polymer layer and it is able to evade the immune system. However, anti-avidin antibodies do generate at some point, probably due to the presence of avidin (or avidin deriving) peptides generated upon NP degradation. Still, the immune response seems weak, so that the antibodies are not strong enough to recognize the protein when protected by the ANANAS PEG layer. This result indicates a "stealth" property of the nanoassembly and is encouraging in view of a potential use of ANANAS as a carrier needing multiple administrations.

Biodistribution, Pharmacokinetics, and Cell Internalization. From the pharmacokinetic and biodistribution point of view, an ideal carrier for parenteral administration should be able to circulate in the bloodstream long enough to reach and diffuse through all tissues and permit deliverance of its cargo to the target site. However, once the target is reached, the carrier should be cleared from the body within a reasonable time. Keeping this in mind, we investigated the *in vivo* biodistribution of PEG-FITC-ANANAS-alexa^{633}. To this end, we used the noninvasive FLuorescence optical Imaging (FLI), a tool that enables longitudinal real-time monitoring of the *in vivo* localization and biodistribution of fluorescent labeling compounds. This technique not only allows to minimize the use of animals according to 3R (reduce, refine, replace) as stated by the Directive 2010/63/EU, but also facilitates an efficient follow-up of each single experimental subject. Therefore, this strategy reduces the gap between humans and animals in

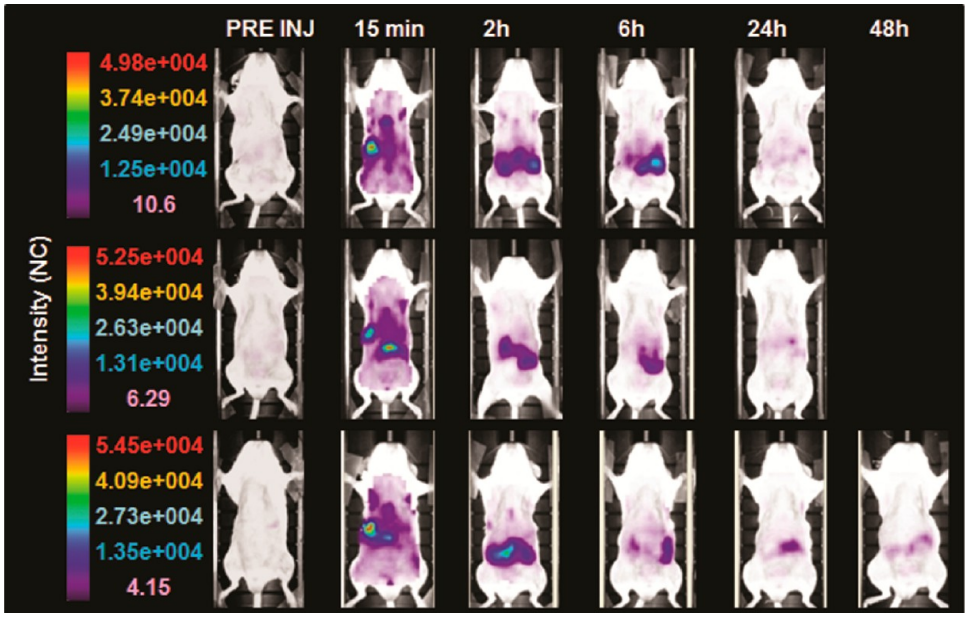

Figure 5. *In vivo* **biodistribution of PEG-FITC-ANANAS-alexa^{633} after iv administration. Representative images acquired before (PRE INJ) administration, and at scheduled time points (15 min, and 2, 6, 24, and 48) after injection. The fluorescence signal intensity, measured as normalized photon counts (NC), is shown as a pseudo-color scale bar. For each mouse, the pseudo-color scale bar is consistent for all images, in order to show relative changes of biodistribution over time. As controls, five animals received the vehicle solution only. The FLI pattern registered in these controls was the same of that of preinjected animals (data not shown).**

terms of investigation procedures, thus increasing the translational level of the research. From a technical point of view, the use of far red fluorophores, as the alexa^{633}, permits relatively deep photon penetration into tissue, avoids the generation of background due to the autofluorescence of tissues and generates a high optical contrast.[51]

The reliability of the FLI based investigation was verified in a preliminary experiment (Figure S-9 in Supporting Information), in which we followed the *in vivo* fate of the monomeric avidin:B−C_6-alexa^{633} (1:1 mol/mol) and avidin:B-(PEG-FITC)$_2$:B−C_6-alexa^{633} (1:1:1 mol/mol/mol) complexes. The results were indeed similar to the pharmacokinetic data obtained through other analytical tools.[28,36,39]

To investigate the pharmacokinetics and biodistribution of PEG-FITC-ANANAS-alexa^{633}, NP solution was administered into the tail vein of 15 healthy NFR mice. Animals were scanned by FLI before and immediately after (15 min) injection, and 2, 6, 24, and 48 h later, to monitor the localization of ANANAS-related fluorescent signal (Figure 5). At each time point, three animals were sacrificed and *ex vivo* NIR analysis of liver, spleen and kidneys was also carried out (Figure 6).

The overall FLI pattern registered was nearly overlapping among the three mice tested, indicating good homogeneity and reproducibility in the particle behavior. The biodistribution information registered is in accordance with the metabolic pattern of clearance observed with other biocompatible nanostructures already used at the clinical level for diagnostic

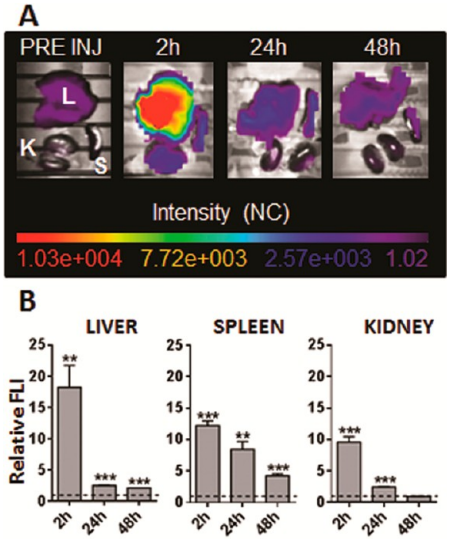

Figure 6. *Ex vivo* **optical imaging analysis. (A) Three mice for each time point (2−24−48 h) after PEG-FITC-ANANAS-alexa^{633} injection were sacrificed, the abdominal organs (L = liver, K = kidneys and S = spleen) were excised and scanned by optical imaging analysis. The intensity of the fluorescent signal, measured as normalized photon counts (NC), is shown as a pseud-ocolor scale bar that is consistent for all images. (B) At each time point, the relative fluorescent intensity (FLI) signal registered from all excised organs was quantified and expressed in the graph as relative FLI. The dashed lines represent the average value of the vehicle treated animals normalized to 1. Data are presented as mean ± SE. The analysis was performed by unpaired Student's *t* test, *$P < 0.05$, **$P < 0.005$, ***$P < 0.0001$ in respect with vehicle-treated mice.**

purposes:[52,53] immediately after injection, the *in vivo* fluorescent signal spread in the whole toraco-abdominal

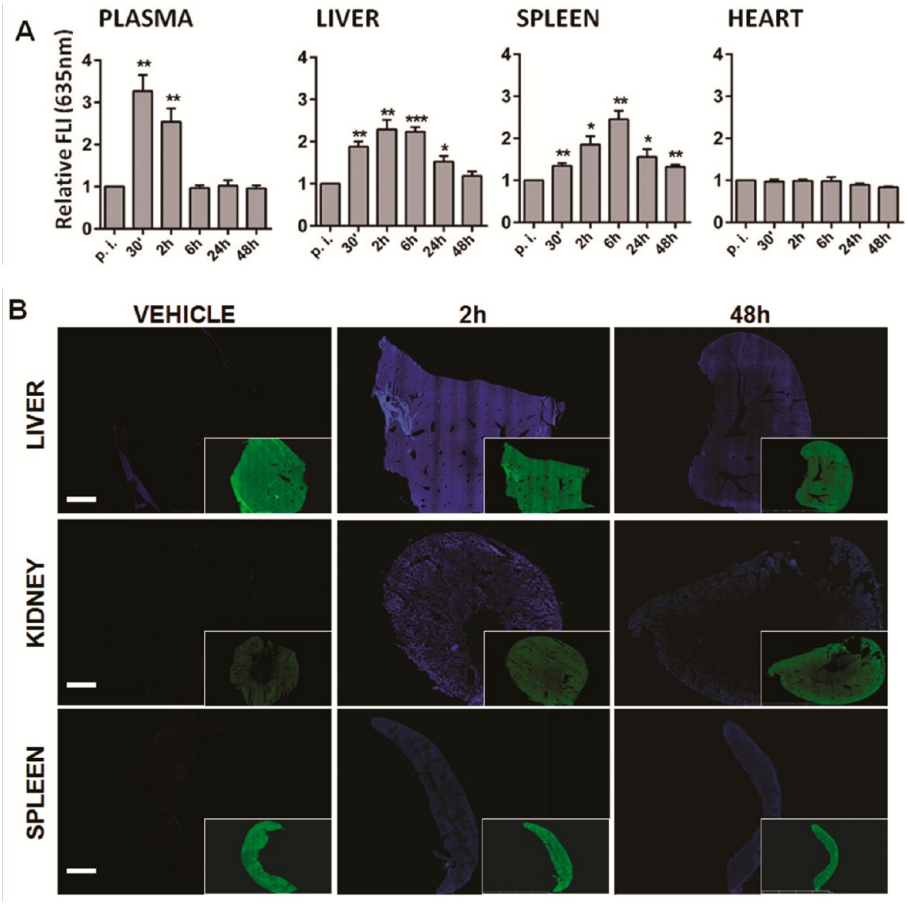

Figure 7. Results of the pharmacokinetic investigation of PEG-FITC-ANANAS-alexa^{633}. (A) Histograms showing the time-course of alexa^{633} associated signal in plasma, liver, kidneys and spleen of NP treated animals. Organs were perfused with PBS before analysis and/or fixation. Fluorescence values were normalized to those measured in non treated animals. (B) Representative sections of liver (upper panels), kidney (middle panels) and spleen (lower panels) from vehicle- (left column) and NP-treated mice, sacrificed 2 h (middle columns) and 48 h (right columns) after administration, as obtained through the nanozoomer instrumentation The alexa^{633}-associated signal (in blue) is absent in vehicle-treated animals (left panels) but is clearly visible in samples from NP-treated animals. On the contrary, a strong tissue autofluorescence in the FITC exciting laser ($\lambda\sim$ 488 nm) channel (green), observable also in the vehicles-treated animals, makes it difficult to appreciate any difference between NP- and vehicle-treated animals at this wavelength. This is in agreement with the *in vivo* analysis, in which no specific signal could be registered by scanning the animals using the laser-associated with fluoresceine (not shown). Scale bar: upper panels, 2 mm; middle and lower panels, 1 mm.

area, with higher intensity levels concentrating in a specific region, probably corresponding to the liver and spleen. Two to six hours after injection, most of the signal had moved toward consistent specific areas of the abdominal region. After 24 h, a dramatic reduction of the overall signal was registered and which was reduced to almost preinjection levels at 48 h. Interestingly, the fluorescent signal plasma permanence registered for the nanoassembly is similar to that observed for the complex monomeric avidin:B-(PEG-FITC)$_2$:B$-$C$_6$-alexa^{633} complex (Supporting Information, Figure S-9). However, the pattern of distribution, accumulation and clearance is slightly different between the two species (*e.g.*, the avidin:B-(PEG-FITC)$_2$:B$-$C$_6$-alexa^{633} complex did not show spleen localization and its signal was eliminated through the kidneys, whereas a much lower signal in the bladder was recorded in NP treated animals), confirming the fact that they are indeed different species.

The relative photon counts measured from liver, spleen and kidneys explanted from the NP-administered animals (Figure 6) are consistent with the *in vivo* analysis: strong signal intensity in organs was registered 2 h after administration, with a peak of fluorescence in the liver.

Twenty-four hours after injection, a marked signal reduction was observed in all organs analyzed, with a kinetics that appears faster in liver and kidneys than in spleen. Two days after administration, the signal had almost completely disappeared from both liver and kidney whereas a lower, but still detectable fluorescence was found in the spleen.

More detailed pharmacokinetic records were obtained in a second set of experiments by measuring spectrophotometrically the fluorescence levels in

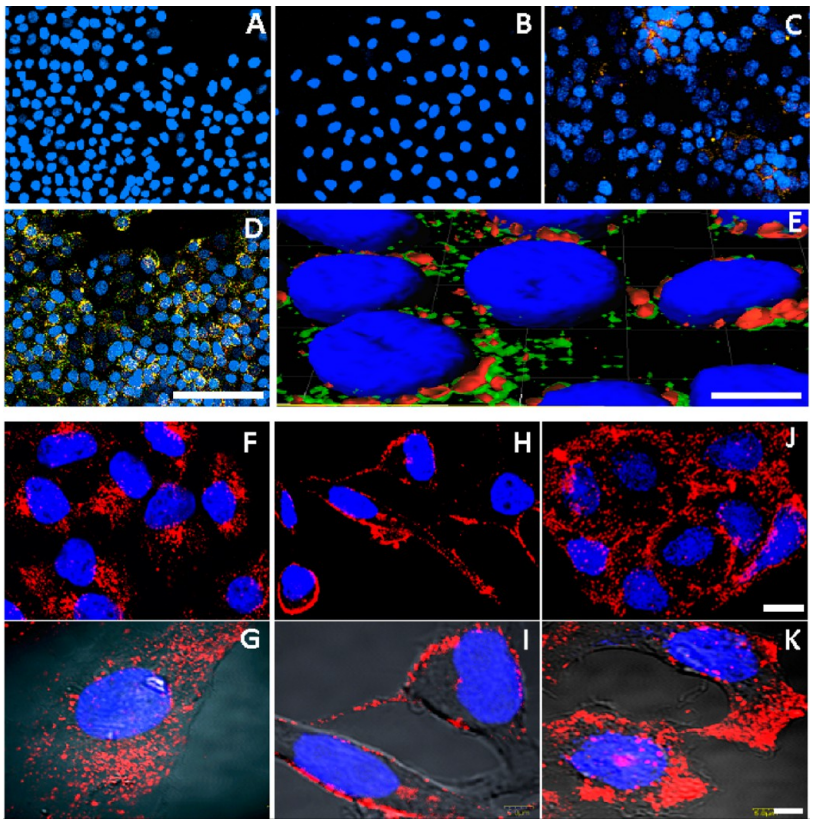

Figure 8. Representative confocal images of HeLa cells incubated with PEG-FITC-ANANAS-alexa^{633} (30 μg/mL in 10% FCS culture medium). Similar results (not shown) were obtained using lower NP concentration (6 μg/mL). Panels A−E show the merge (red for alexa^{633}, green for FITC, yellow for merged alexa^{633}/FITC) among the fluorescent channels associated to the NPs and the nuclei (in blue after staining with Hoechst 33258, 2 μg/mL). A representative image of control cells (treated with PBS only) is reported in panel A. In panels B,−D, cells treated with NPs for 2 h (B), 6 h (C) and 24 h (D) can be observed. In panel E, a 3D reconstruction of 24 h treated cells is reported. Hoechst 33258 labeled nuclei are visualized in blue, while both green (FITC) and red (alexa^{633}) signals are associated with ANANAS. Panels F−K display representative low (F, H, and J) and high (G, I, and K) magnification images of cells upon 24 h incubation with NPs in basal conditions (F−G), or in presence of chloropromazine (20 μg/mL) (H and I) or amyloride 1 mM (J and K). Hoechst 33258 labeled nuclei are visualized in blue, while both green (FITC) and red (alexa^{633}) signals are associated to ANANAS. In physiological conditions, the ANANAS spread homogenously in the cytoplasm of all cells (F), showing a punctuate pattern of vesicle-like staining (G). Treatment with chloropromazine leads to NP accumulation around the cell periphery (H) and the merge between fluorescence and nomarski acquisitions reveals that almost all of the spots are confined in proximity of the plasma membrane (I). Amyloride treatment did not show relevant inhibition of NP uptake and significant entry of NP can be observed at this time-point (J and K). Scale bars: (A−D) 100 μm; (E) 10 μm; (F, H and J) 20 μm; (G, I and K) 5 μm.

plasma, liver, spleen and kidney homogenates at different time-points after administration (Figure 7). A 30 min time-point was included in this case, in order to improve the analysis of the early phase of the distribution and elimination processes.

The pharmacokinetics data registered from the supernatants of centrifuged organ homogenates (Figure 7A) demonstrate the existence of NPs circulating freely in the bloodstream for more than two hours. Between 30 to 120 min, the plasma alexa^{633}-associated fluorescence decreased less than 40% and six hours after administration, the signal intensity was reduced to almost preinjection levels. Concurrently, the alexa^{633}-signal moved into the *metabolic* organs, with a *t*-max between 2 and 6 h in the liver and ≥6 h in the spleen. No changes in the fluorescence levels of hearth homogenates, a well perfused *nonmetabolic* organ, were registered along the whole experiment, during which the heart-associated signal remained similar to that of pretreated mice.

To verify the pattern of signal associated with NP within each organ tissue, a large number of sections from liver, spleen and kidney obtained from animals sacrificed 2 and 48 h after administration was acquired with Nanozoomer HT 2.0 scanner with fluorescence optics (Figure 7B).

In agreement with the pharmacokinetic studies, the NP-associated signal was high 2h after administration and markedly reduced after 48 h (even if still visible). Signal decay was less pronounced in spleen than in other organs, confirming the information gained by the Optix instrumentation. The Nanozoomer analysis allowed a convenient and rapid scan of the organs in their whole volume, permitting to understand the overall distribution of the particles in the organs: heterogeneous accumulation of ANANAS was

observed in kidney and spleen sections and observational results suggest that in kidneys the NPs accumulate close to the glomeruli endothelial structures, while in spleen they localize in the red pulp (likely in resident marcrophages). On the other hand, in liver, the alexa^{633} signal was uniformly spread in the entire parenchyma and analysis at higher resolution through confocal microscopy (Figure S-10 in Supporting Information) showed that the NPs were almost homogeneously diffused around the nuclei in a spot-like staining. The peripheral distribution of separate spots and the presence of signal around the nuclei strongly suggests that an active process of internalization occurred by a mechanism of nanoparticle-dependent vesicles formation. The ability of ANANAS to internalize cells was further demonstrated in an *in vitro* test in which NP accumulation in HeLa cells upon incubation for 2, 6, and 24 h was monitored by confocal microscopy. As shown in Figure 8, cell association and internalization occur quite efficiently, even if at a relatively slow pace. The kinetics observed along this experiment, which has been carried out in the presence of serum, supports the *in vivo* observation that the ANANAS can efficiently internalize cells, provided they have the opportunity to stay in contact with them for some time. Upon internalization, the NPs localize primarily within the cytoplasm (Figure 8E,G), where they appear as separate spots, resembling clusters of internalization vesicles. Treatment with chloropromazine, a selective inhibitor of clathrin-dependent endocytosis, strongly reduces NP entry (Figure 8H,I), whereas incubation with amyloride, which selectively inhibits macropinocytosis, does not lead to significant alteration on NP uptake for at least 24 h (Figure 8J,K). This strongly suggests that a vesicle-dependent process of endocytosis occurs (see single fluorescent spots in Figure 8F,G), secondary to clathrin-dependent vesicle formation (see the lack of NP internalization in Figure 8H,I). This is in agreement with other studies showing that nanomaterials can be uptaken by a large variety of cells through a "troyan horse"-like mechanism.

CONCLUSIONS

The multimodal approach adopted in this study allowed us to disclose quali-quantitatively the *in vivo* fate of the dually fluorescent ANANAS formulation here optimized. Altogether, the information obtained consistently indicate that, when mixed with biological fluids, the NPs maintain their assembled conformation and are slowly degraded by a combination of mechanisms, including avidin disassembly from the core and slow detachment of the biotinylated elements. *In vivo*, these phenomena occur concomitantly to NP accumulation in liver and spleen, probably also secondary to opsonization by plasma proteins. The formulation does not have any special tropism other than that for normal scavenging organs and its fate is in line with that registered for other biocompatible NPs. Although the particles have the ability to penetrate cells, this property neither induces their accumulation nor avoids their clearance and/or their degradation. Indeed, the *in vitro* tests showed that cell internalization occurs rather slowly, so that some time of contact with the target cells is necessary. As a consequence, unless a targeting element is inserted in the NP composition, cell penetration *in vivo* can occur only in the scavenging organs and no accumulation occurs elsewhere. As such, the lack of accumulation observed provides an important suggestion for the development of this nanodevice for diagnostic and/or drug-delivery application. On this matter, we would like to note that a major reason for FDA approval of the first nanoliposomal doxorubicin (DOXIL) was its limited heart availability/accumulation, with consequent reduced cardiotoxicity.

The results show that the formulation here investigated represents an advancement in avidin-based targeting technologies: with respect to monomeric avidin, it displays more favorable pharmacokinetic properties, since circulating NPs can be detected for more than 2 h after iv administration. The NP plasma residence is similar to that of the PEGylated form of the protein, with the important advantage of having a much higher payload for biotinylated active moieties and being less immunogenic. Since antibodies capable to recognize the assembled particles do not form at least after two repeated administrations, this formulation could be greatly advantageous for treatments that necessitate multiple administrations.

With respect to the NP plasma residence, it is important to note that the carbohydrate portion in avidin is known to be responsible for increasing the protein liver localization, but only when saturated with biotin.[28] Considering that most of the avidin in a functional ANANAS formulation is biotinylated, it is possible that the NP liver tropism here observed may, at least in part, be related to the protein glycosidic portion. If so, and if necessary, the NP plasma residence could be further prolonged by replacing the native protein with its nonglycosylated analogue.[54]

Overall, the results are encouraging toward a future evaluation of the NP fate when in contact with leaky vascularized inflamed or cancer tissues, and/or to test if targeted particles can localize into desired tissues or body districts. Ultimately, the theranostic applicability of the system, once functionalized with targeting elements, will depend on its ability to penetrate and be retained into target tissues. In this context, the cell internalizing ability observed through both the *ex vivo* and *in vitro* confocal microscopy analyses suggests that it is possible to carry the bioactive cargoes also inside the cells. Nonetheless, since the biotinylated

elements slowly detach from the core particles, similarly biotinylated bioactive agents (as, for example, drugs), if loaded onto a (targeted) ANANAS, would likely detach from the particles, once these have reached their final body destination. In this respect, it has to be pointed out that if one would like to use the ANANAS as a drug delivery system rather than a diagnostic tool, the linker between the bioactive compound and the NP-tethering biotin should be further engineered to favor local release of the carried moiety in its active form. For example, depending on the biochemical properties of the target environment, the use of pH, cathepsin or temperature sensitive bonds and/or self-immolative spacers can be envisioned.[55−58]

Finally, it is worth mentioning that the biodistribution and pharmacokinetic data were generated taking advantage of the NIR fluorescence alexa^{633}-related information. Although in the formulation investigated this fluorophore occupies less than 20% of the total available BBS (and much less % of the total surface area available for functionalization), the signal generated was high enough to allow quantitative analysis by means of the noninvasive Optix instrumentation, suggesting that, if necessary, the amount of fluorophore could be further reduced without losing sensitivity. This permits a great formulation freedom when seeking more complex functional assemblies—containing, for example, drugs, targeting or cell internalizing moieties—which, in principle, could still be tested through the same noninvasive tools as those used here.

Last but not least, we would like to note the unique mode of ANANAS assembly, which allows to generate functional formulations with stoichiometrically controlled composition in "one-pot" reactions. This permits envisioning the use of this technology not only as a *per se* theranostic tool, but also as a general platform to test the efficacy of functional elements (as, for example, putative tissue-targeting or cell-internalizing moieties) and to establish dose/response relationships that are of general interest for the development of any nanoparticle-based biomedical tool.

METHODS

Materials and Instrumentation. Avidin was purchased from Belovo chemical (Belgium). Plasmid pEGFP-C1, 4.7 kb (used for the ANANAS core preparation), was from Clontech; anti-mouse-HRP was from Millipore; 3,3′,5,5′-tetramethylbenzidine (TMB) was purchased from KPL (Gaithersburg, MD, USA). Ninety-six-well High binding Corning EIA/RIA plates, and all other reagents were from Sigma Aldrich (St. Louis, MO, USA). NAP10 gravity G25 gel permeation columns were purchased from GE Healthcare. Fast Permeation Liquid Chromatography (FPLC) analyses were performed using an AKTA purifier 10 (GE Healthcare) apparatus, equipped with a UV−vis detector and a Superose 6 (10/300 GL) column. UV−vis analyses were performed on a Varian Cary 50 UV−vis spectrophotometer (Varian, Inc., Palo Alto, CA, USA). Dynamic light scattering measurements were performed using a Malvern Zetasizer NANO ZS (Malvern Instruments Ltd., Worcestershire, United Kingdom). ELISA Microplate absorbance was measured with a Multiskan FC microplate reader (Thermo Fisher Scientific, Waltham, MA, USA). Fluorescence spectroscopy data were recorded using a JASCO FP 6200 fluorimeter. A 2300 Multilabel Plate Reader spectrophotofluorimeter (Perkin-Elmer, Boston, MA, USA) was used to quantify the ANANAS associated fluorescence in the pharmacokinetics experiments. Electron microscopy images were obtained with an Energy Filter Transmission Electron Microscope (EFTEM, ZEISS LIBRA 120) equipped with YAG scintillator slow scan CCD camera. Before image acquisition, a PEG-FITC-ANANAS-alexa^{633} solution in ddH_2O was placed to dry overnight on a 100 mesh Formvar/carbon coated copper grid (EMS, Hatfield, PA, USA).

Nanoparticle Preparation and Characterization. The synthesis of the two ω-FITC labeled biotin-PEG derivatives (compounds **4** and **6** and of biotin-C_6-alexa^{633} (compound **7**) is described in the Supporting Information. All NPs were prepared on the basis of a previously published procedure.[13] In the **preformulation studies**, 'Core' FITC-labeled ANANAS were prepared by mixing avidin, compound **6** (Figures 1 and 2) and plasmid DNA at selected molar ratios. In this preparation, the avidin BBS: biotin-PEG derivative molar ratio was 1:0.25. After stabilization, particles were purified from excess of avidin by ultrafiltration (Millipore PVDF membranes, cutoff 100 kDa) or gel permeation chromatography eluting the sample in 10 mM phosphate, 150 mM NaCl, pH 7.4 buffer (PBS) using a Sepharose 6-FF column on a FPLC system (AKTA purifier, GE Healthcare). The eluted particles were stored at 4 °C until further use. The resulting NPs were characterized by dynamic light scattering, UV−vis and fluorescence spectroscopy. The number of fluorescein molecules attached to the purified particles was measured from the UV−vis spectra, on the basis of the 280 nm (avidin, DNA and fluorescein) and 495 nm (fluorescein only) absoption values.

Maximal NP PEG loading capability was assessed by mixing the 'core' particles with molar excesses (with respect to the theoretically available BBS) of either compounds 4 or 6 in PBS. After 1 h incubation, particles were purified by size exclusion chromatography and the number of fluorophores linked was quantified by specrophotometry as above indicated.

The final **B−C_6-alexa^{633}-B-PEG-FITC labeled NP** formulation used for the *in vivo* studies **(PEG-FITC-ANANAS-alexa^{633})** was obtained from a highly FITC-PEGylated ANANAS NP prepared as above using an avidin-BBS:biotin PEG derivative molar ratio of 1:0.46. After purification and UV−vis characterization, the nanoassembly was added of an excess of B−C_6-alexa^{633} (compound **7**). After 30 min incubation, nanoassemblies were purified by gel permeation chromatography as described above and analyzed by DLS, UV−vis and fluorescence spectroscopy. The number of fluorophores attached to the purified particles was measured from the UV−vis spectrum, on the basis of the 280 nm (avidin, DNA and fluorescein) and 495 nm (fluorescein only) and 631 nm (alexa^{633}) absorption values.

Stability of PEG-FITC-ANANAS-alexa^{633} in Serum and Organ Homogenates. Tissues homogenates and plasma were obtained according to the standardized procedures described by our group.[50] Briefly, liver, spleen and plasma were harvested. Tissues were homogenized in 5 mM PBS, pH 7.4, in a 1:4 (w:v) ratio and centrifuged at 9000*g* for 10 min at 4 °C. The supernatant was collected and stored at −20 °C until used.

Stability through Gravity G25 Chromatograpy Analysis. Solutions of PEG-FITC-ANANAS-alexa^{633} (120 μg/mL in PBS) or B−C_6-alexa^{633} were mixed with 0.1 vol of plasma, organ homogenates (spleen and liver) obtained as above, or PBS as a control. At scheduled times, samples were centrifuged (15 000 rpm (16 600*g*), 2 min, 4 °C) and the supernatants were either eluted through a gravity G25 medium (NAP10, GE Healthcare) or analyzed by gel permeation chromatography using an Akta purifier (GE) FPLC apparatus integrated with a Superose 6

column, using PBS as eluant. In the case of the NAP analysis, this procedure was carried out on mixtures as prepared and after incubation at 37 °C for 16, 48 and 72 h. The eluted fractions (0.5 mL) were analyzed by UV−vis and fluorescence Spectroscopy (λ_{exc} 632 nm, λ_{em} 647 nm, slidts 5 nm, high sensitivity). For quantitative analysis, each sample elution profile was compared to that of PEG-FITC-ANANAS-alexa^{633}, B−C_6-alexa^{633} and alexa^{633}-COOH (Supporting Information, Figure S-7). As a control, B−C_6-alexa^{633} was also treated and analyzed in the same way. FPLC analysis was carried out on mixtures as prepared and after 15 h incubation at 37 °C. Samples were eluted with PBS buffer at 0.5 mL/min, and elution was monitored at 280, 495, and 631 nm.

***In Vivo* Experiments.** Procedures involving animals and their care were conducted in conformity with the institutional guidelines that are in compliance with national (D.L. no. 116, G.U., suppl. 40, 18 Febbraio 1992; Circolare no. 8, G.U., 14 Luglio 1994) and international (EEC Council Directive 86/609, OJL 358, 1, 12 December 1987; Guide for the Care and Use of Laboratory Animals, U.S. National Research Council, 1996) laws and policies.

Immunogenicity. Repeated (three) subcutaneous injections of PEG-FITC-ANANAS-alexa^{633}, avidin, and avidin:B-(PEG-FITC)$_2$ (1:1) complex diluted in PBS (60 μg/mL) were administered in three separate animal groups (N = 3) every two weeks. Plasma was collected one week after each administration and stored at −20 °C until analysis. At the end of the experiment, the antibody titer against each avidin form was measured in all samples. A conjugate between BSA and biotin-PEG$_{5kDa}$ (B-PEG-BSA) was obtained by classic bioconjugation procedures using biotin-PEG$_{5kDa}$-NHS (laysan Bio). NUNC maxisorp 96-well microplates were incubated overnight with B-PEG-BSA, (4 °C) (4 μg/mL) in 0.05 M $NaHCO_3$, pH 9.3. After blocking with PBS containing 0.05% of Tween 20 (PBST) and 0.3% BSA, avidin, avidin−biotin-PEG and PEG-FITC-ANANAS coated wells were generated by incubating each of the above reagents (all 4 μg/mL in PBST, 2 h, 37 °C) with the B-PEG-BSA-coated wells. Mice sera were serially diluted (from 1:100 to 1:1 000 000) with PBST + 0.1% BSA) and were incubated in the above wells for 1 h at 37 °C. The relative level of all antigen-specific mouse IgGs was compared by the signal generated after anti-mouse-HRP incubation (diluted in PBST + 0.1% BSA 1 h, 37 °C) and 10 min of TMB (50 μL/well) development, followed by stopping the reaction by the addition of 50 μL/well of 0.5 M H_2SO_4 and absorbance readout at 450 nm. All samples were tested in triplicate. A NP formulation containing slightly less PEG$_{5kDa}$-FITC chains than the one injected in mice (600 instead of 700) was used in these experiments to ensure the assembly surface tethering through the B-PEG-BSA anchoring element).

***In Vivo* and *ex Vivo* Fluorescence Imaging.** *In vivo* whole body fluorescence imaging was performed longitudinally on mice injected intravenously with PEG-FITC-ANANAS-alexa^{633} (140 μg/mL in PBS + 0.05% Tween 20) using the Explore Optix System (ART Advanced Research Technologies, Montreal, Canada), and a fixed pulsed laser diode as an illumination source. Before imaging, animals were anesthetized with a continuous flow of 5% isoflurane/oxygen mixture and placed on their back on a heated (37 °C) pad inside the camera box and 2−3% isoflurane anesthesia was maintained using a nose cone delivery system for the duration of image acquisition. For each animal, a region of interest (ROI) of the ventral whole body was chosen with a step size of 2 mm and a spot size of 1 mm. Excitation was performed with a 635 nm pulsing laser and emission was detected with a 650 nm long pass filter. Subsequently, a photomultiplier tube (PMT) coupled to a time correlated single photon counting system collects the emitted light, allowing detection of fluorescent signal. Light emission was recorded as pseudo-color images. Overlay of gray scale (body reference photograph) and pseudo-color images allowed localization of fluorescent signal. Mice injected with PEG-FITC-ANANAS-alexa^{633} were scanned before injection and immediately after 15 min and 2, 6, 24, and 48 h later. For each time point, three animals were sacrificed, and their abdominal organs (liver, spleen and kidneys) were removed and scanned for the *ex vivo* fluorescence imaging. A ROI was designed around each organ and light/photon emission in the selected ROI was quantified as total photon counts using Optiview software (version 2.02.00; ART Advanced Research Technologies). At each time point, the mean FLI signal values detected around liver, spleen and kidneys were measured and expressed as relative values to those measured from PBS-treated animals.

Statistical Analysis. All data were analyzed with the use of GraphPad Prism software (version 5.03). In particular, the differences in fluorescent intensity between multiple groups have been evaluated using a one way ANOVA test followed by the Bonferroni's test. Data were expressed as the mean ± standard deviation (SD). The differences were considered statistically significant at a level of $P < 0.05$.

Pharmacokinetic Study through Fluorescence Titration of Plasma and Organ Homogenates. A total of 18 animals were used, and 3 of these kept as control. The remaining 15 were intravenously treated with a solution of PEG-FITC-ANANAS-alexa^{633} (127.8 μg/mL (w/v) in PBS + 0.05% Tween 20. At each time point (30 min, 2, 6, 24, and 48 h), three animals were sacrificed by cervical dislocation. Fresh blood was collected from the retroorbital plexus and kept into EDTA (0.5 M, pH 8) pretreated tubes at 4 °C for about 30 min. To separate plasma from entire blood, the collected samples were centrifuged for 15 min at 1500*g*. The supernatant (plasma) was collected and aliquots were immediately frozen. Tissues were homogenized as described above. Before use, homogenates were diluted 1:10 (v/v) with distilled water, centrifuged at 1100*g* for 10 min at 25 °C and the supernatant recovered in order to obtain transparent solutions. Spectrophotofluorimetric analyses were conducted to correlate the fluorescence intensity (FI) measured into the collected samples to the presence of PEG-FITC-ANANAS-alexa^{633}. FI was determined at λ_{exc} = 470 nm and λ_{em} = 520 nm for FITC and at λ_{exc} = 600 nm and λ_{em} = 670 nm for alexa^{633} using an 2300 Multilabel Plate Reader spectrophotofluorimeter (Perkin-Elmer, Boston, MA, USA) with a standard 96 wells black plate with a transparent bottom (ProxiPlate-96, Perking Elmer). The fluorescence intensity of all samples was compared to that measured from blank (non treated) animals.

***In Vitro* Cell Internalization Assay.** HeLa cells were seeded on round glass slides in 24-well plates at the concentration of 10 000 cell/well in culture medium (DMEM, 10% fetal bovine serum, 2 mM L-glutamine, 100 U penicillin/0.1 mg/mL streptomycin) and incubated at 37 °C, 5% CO_2, for 24 h. Culture medium was then removed and replaced with a suspension PEG-FITC-ANANAS-alexa^{633} (30 μg/mL) in culture medium for 2, 6, and 24 h, respectively. At the end of incubation, cells were fixed with 4% paraformaldehyde in PBS for 40 min and nuclei were stained with Hoechst 33258 (2 μg/mL in PBS, incubation for 40 min). Glass slides were mounted on cover glass slides with 2−3 drops of Fluormont and stored at 4 °C. Samples were then analyzed with an Olympus Fluoview microscope BX61 with confocal system FV500, equipped with specific lasers λ_{exc} = 405 nm, λ_{exc} = 488 nm, and λ_{exc} = 635 nm to visualize Hoechst 33258, FITC, and alexa^{633}, respectively. Two dimensional and three-dimensional images (z stack reconstruction of one focal plane acquisition every 0.2 μm on the z axis) were acquired. Images were pseudo-colored (blue for Hoechst 33258, green for FITC and AF 488, red for alexa^{633}), and the signal obtained from the three channels was automatically merged by Olympus fluoview software. 3-D reconstruction was performed using Imaris 5.0 (Bitplane) software. In a separate experiment and in order to investigate on the mechanism of NP uptake, cells were co-incubated for 24 h as above with PEG-FITC-ANANAS-alexa^{633} (30 μg/mL) in the presence of chloropromazine (final concentration, 20 μg/mL) or amyloride (final concentration, 1 mM). Fixation and visualization were performed as above-described.

Conflict of Interest: The authors declare no competing financial interest.

Acknowledgment. This project was funded by the "Progetto di Ateneo" of the University of Padova n.CPDA072372. Authors are greatly indebted to Dr. Rosanna Piccirillo for her critical reading and her suggestions. A particular thanks to Dr. Stefano Pezzati Eng. and Dr. Annamaria Mauro from Hamamtsu Photonics Italia for the support in acquiring images.

Supporting Information Available: Synthesis and characterization of biotinylated elements; DLS size and ζ-potential the final assemblies, biodistribution of individual NP components through FLI; *ex vivo* histological analyses. This material is available free of charge *via* the Internet at http://pubs.acs.org.

REFERENCES AND NOTES

1. Hrkach, J.; Von Hoff, D.; Ali, M. M.; Andrianova, E.; Auer, J.; Campbell, T.; De Witt, D.; Figa, M.; Figueiredo, M.; Horhota, A.; *et al.* Preclinical Development and Clinical Translation of a PSMA-Targeted Docetaxel Nanoparticle with a Differentiated Pharmacological Profile. *Sci. Transl. Med.* **2012**, *4*, 128–139.
2. Zamboni, W. C.; Torchilin, V.; Patri, A. K.; Hrkach, J.; Stern, S.; Lee, R.; Nel, A.; Panaro, N. J.; Grodzinski, P. Best Practices in Cancer Nanotechnology: Perspective from Nci Nanotechnology Alliance. *Clin. Cancer Res.* **2012**, *18*, 3229–3241.
3. Bourzac, K. Carrying Drugs. *Nature* **2012**, *491*, S58–60.
4. Winter, P. M.; Neubauer, A. M.; Caruthers, S. D.; Harris, T. D.; Robertson, J. D.; Williams, T. A.; Schmieder, A. H.; Hu, G.; Allen, J. S.; Lacy, E. K.; *et al.* Endothelial Alpha(V)Beta(3) Integrin-Targeted Fumagillin Nanoparticles Inhibit Angiogenesis in Atherosclerosis. *Arterioscler., Thromb., Vasc. Biol.* **2006**, *26*, 2103–2109.
5. Zhou, H. F.; Yan, H.; Senpan, A.; Wickline, S. A.; Pan, D.; Lanza, G. M.; Pham, C. T. Suppression of Inflammation in a Mouse Model of Rheumatoid Arthritis Using Targeted Lipase-Labile Fumagillin Prodrug Nanoparticles. *Biomaterials* **2012**, *33*, 8632–8640.
6. Sharrna, P.; Brown, S.; Walter, G.; Santra, S.; Moudgil, B. Nanoparticles for Bioimaging. *Adv. Colloid Interface Sci.* **2006**, *123*, 471–485.
7. Mansilla, E.; Marin, G. H.; Nunez, L.; Drago, H.; Sturla, F.; Mertz, C.; Rivera, L.; Ichim, T.; Riordan, N.; Raimondi, C. The Lysosomotropic Agent, Hydroxychloroquine, Delivered in a Biodegradable Nanoparticle System, Overcomes Drug Resistance of B-Chronic Lymphocytic Leukemia Cells *in Vitro*. *Cancer Biother. Radiopharm.* **2010**, *25*, 97–103.
8. Islam, T.; Josephson, L. Current State and Future Applications of Active Targeting in Malignancies Using Superparamagnetic Iron Oxide Nanoparticles. *Cancer Biomarkers* **2009**, *5*, 99–107.
9. Kelkar, S. S.; Reineke, T. M. Theranostics: Combining Imaging and Therapy. *Bioconjugate Chem.* **2011**, *22*, 1879–1903.
10. Stefanick, J. F.; Ashley, J. D.; Kiziltepe, T.; Bilgicer, B. A Systematic Analysis of Peptide Linker Length and Liposomal Polyethylene Glycol Coating on Cellular Uptake of Peptide-Targeted Liposomes. *ACS Nano* **2013**, *7*, 2935–2947.
11. Morpurgo, M.; Facchin, S.; Pignatto, M.; Silvestri, D.; Casarin, E.; Realdon, N. Characterization of Multifunctional Nanosystems Based on the Avidin-Nucleic Acid Interaction as Signal Enhancers in Immuno-Detection. *Anal. Chem.* **2012**, *84*, 3433–3439.
12. Morpurgo, M.; Radu, A.; Bayer, E. A.; Wilchek, M. DNA Condensation by High-Affinity Interaction with Avidin. *J. Mol. Recognit.* **2004**, *17*, 558–566.
13. Pignatto, M.; Realdon, N.; Morpurgo, M. Optimized Avidin Nucleic Acid Nanoassemblies by a Tailored Pegylation Strategy and Their Application as Molecular Amplifiers in Detection. *Bioconjugate Chem.* **2010**, *21*, 1254–1263.
14. Wilchek, M.; Bayer, E. A. The Avidin-Biotin Complex in Bioanalytical Applications. *Anal. Biochem.* **1988**, *171*, 1–32.
15. Abelson, J.; Simon, M.; Wichek, M.; Bayer, E. A., Eds. *Avidin-Biotin Technology*; Methods in Enzymology; Academic Press: San Diego, CA, 1990; Vol. 184.
16. Bratthauer, G. L. The Avidin-Biotin Complex (Abc) Method and Other Avidin-Biotin Binding Methods. *Methods Mol. Biol.* **1999**, *115*, 203–214.
17. Lesch, H. P.; Kaikkonen, M. U.; Pikkarainen, J. T.; Yla-Herttuala, S. Avidin-Biotin Technology in Targeted Therapy. *Expert Opin. Drug Delivery* **2010**, *7*, 551–564.
18. Yan, H.; Jiang, W. M.; Zhang, Y. X.; Liu, Y.; Wang, B.; Yang, L.; Deng, L. H.; Singh, G. K.; Pan, J. Novel Multi-Biotin Grafted Poly(Lactic Acid) and Its Self-Assembling Nanoparticles Capable of Binding to Streptavidin. *Int. J. Nanomed.* **2012**, *7*, 457–465.
19. Pulkkinen, M.; Pikkarainen, J.; Wirth, T.; Tarvainen, T.; Haapa-aho, V.; Korhonen, H.; Seppala, J.; Jarvinen, K. Three-Step Tumor Targeting of Paclitaxel Using Biotinylated Pla-Peg Nanoparticles and Avidin-Biotin Technology: Formulation Development and *in Vitro* Anticancer Activity. *Eur. J. Pharm. Biopharm.* **2008**, *70*, 66–74.
20. Ting, S. R.; Nguyen, T. L.; Stenzel, M. H. One Pot Synthesis of Surface Pegylated Core-Shell Microparticles by Suspension Polymerization with Surface Enrichment of Biotin/Avidin Conjugation. *Macromol. Biosci.* **2009**, *9*, 211–220.
21. Li, S.; Liu, H. N.; He, N. Y. Covalent Binding of Streptavidin on Gold Magnetic Nanoparticles for Bead Array Fabrication. *J. Nanosci. Nanotechnol.* **2010**, *10*, 4875–4882.
22. Wang, Y.; Liu, X. R.; Nakamura, K.; Chen, L.; Rusckowski, M.; Hnatowich, D. J. *In Vivo* Delivery of Antisense Morf Oligomer by Morf/Carrier Streptavidin Nanoparticles. *Cancer Biother. Radiopharm.* **2009**, *24*, 573–578.
23. Gbadamosi, J. K.; Hunter, A. C.; Moghimi, S. M. Pegylation of Microspheres Generates a Heterogeneous Population of Particles with Differential Surface Characteristics and Biological Performance. *FEBS Lett.* **2002**, *532*, 338–344.
24. Schiestel, T.; Brunner, H.; Tovar, G. E. M. Controlled Surface Functionalization of Silica Nanospheres by Covalent Conjugation Reactions and Preparation of High Density Streptavidin Nanoparticles. *J. Nanosci. Nanotechnol.* **2004**, *4*, 504–511.
25. Maeda, Y.; Yoshino, T.; Takahashi, M.; Ginya, H.; Asahina, J.; Tajima, H.; Matsunaga, T. Noncovalent immobilization of streptavidin on in vitro- and in vivo-biotinylated bacterial magnetic particles. *Appl. Environ. Microbiol.* **2008**, *74*, 5139–5145.
26. Chirra, H. D.; Sexton, T.; Biswal, D.; Hersh, L. B.; Hilt, J. Z. Catalase-Coupled Gold Nanoparticles: Comparison between the Carbodiimide and Biotin-Streptavidin Methods. *Acta Biomater.* **2011**, *7*, 2865–2872.
27. Erdem, A.; Sayar, F.; Karadeniz, H.; Guven, G.; Ozsoz, M.; Piskin, E. Development of Streptavidin Carrying Magnetic Nanoparticles and Their Applications in Electrochemical Nucleic Acid Sensor Systems. *Electroanalysis* **2007**, *19*, 798–804.
28. Schechter, B.; Silberman, R.; Arnon, R.; Wilchek, M. Tissue Distribution of Avidin and Streptavidin Injected to Mice - Effect of Avidin Carbohydrate, Streptavidin Truncation and Exogenous Biotin. *Eur. J. Biochem.* **1990**, *189*, 327–331.
29. De Santis, R.; Leoni, B.; Rosi, A.; Albertoni, C.; Forni, G.; Cojoca, R.; Iezzi, M.; Musiani, P.; Paganelli, G.; Chinol, M.; *et al.* Avidinox for Highly Efficient Tissue-Pretargeted Radionuclide Therapy. *Cancer Biother. Radiopharm.* **2010**, *25*, 143–148.
30. Paganelli, G.; De Cicco, C.; Ferrari, M. E.; Carbone, G.; Pagani, G.; Leonardi, M. C.; Cremonesi, M.; Ferrari, A.; Pacifici, M.; Di Dia, A.; *et al.* Intraoperative Avidination for Radionuclide Treatment as a Radiotherapy Boost in Breast Cancer: Results of a Phase Ii Study with (90)Y-Labeled Biotin. *Eur. J. Nucl. Med. Mol. Imaging* **2010**, *37*, 203–211.
31. Paganelli, G.; Ferrari, M.; Cremonesi, M.; De Cicco, C.; Galimberti, V.; Luini, A.; Veronesi, P.; Fiorenza, M.; Carminati, P.; Zanna, C.; *et al.* Iart: Intraoperative Avidination for Radionuclide Treatment. A New Way of Partial Breast Irradiation. *Breast* **2007**, *16*, 17–26.
32. Paganelli, G.; Ferrari, M.; Ravasi, L.; Cremonesi, M.; De Cicco, C.; Galimberti, V.; Sivolapenko, G.; Luini, A.; De Santis, R.; Travaini, L. L.; *et al.* Intraoperative Avidination for Radionuclide Therapy: A Prospective New Development to Accelerate Radiotherapy in Breast Cancer. *Clin. Cancer Res.* **2007**, *13*, 5646s–5651s.
33. Petronzelli, F.; Pelliccia, A.; Anastasi, A. M.; Lindstedt, R.; Manganello, S.; Ferrari, L. E.; Albertoni, C.; Leoni, B.; Rosi, A.; D'Alessio, V.; *et al.* Therapeutic Use of Avidin Is Not Hampered by Antiavidin Antibodies in Humans. *Cancer Biother. Radiopharm.* **2010**, *25*, 563–570.

34. Paganelli, G.; Chinol, M.; Maggiolo, M.; Sidoli, A.; Corti, A.; Baroni, S.; Siccardi, A. G. The Three-Step Pretargeting Approach Reduces the Human Anti-Mouse Antibody Response in Patients Submitted to Radioimmunoscintigraphy and Radioimmunotherapy. *Eur. J. Nucl. Med.* **1997**, *24*, 350–351.
35. Bubb, M. O.; Green, F.; Conradie, J. D.; Tchernyshev, B.; Bayer, E. A.; Wilchek, M. Natural Antibodies to Avidin in Human Serum. *Immunol. lett.* **1993**, *35*, 277–280.
36. Yao, Z. S.; Zhang, M. L.; Sakahara, H.; Nakamoto, Y.; Higashi, T.; Zhao, S.; Sato, N.; Arano, Y.; Konishi, J. The Relationship of Glycosylation and Isoelectric Point with Tumor Accumulation of Avidin. *J. Nucl. Med.* **1999**, *40*, 479–483.
37. Yao, Z. S.; Zhang, M. L.; Sakahara, H.; Saga, T.; Arano, Y.; Konishi, J. Avidin Targeting of Intraperitoneal Tumour Xenografts. *J. Natl. Cancer. Inst.* **1998**, *90*, 25–29.
38. Chinol, M.; Casalini, P.; Maggiolo, M.; Canevari, S.; Omodeo, E. S.; Caliceti, P.; Veronese, F. M.; Cremonesi, M.; Chiolerio, F.; Nardone, E.; *et al.* Biochemical Modifications of Avidin Improve Pharmacokinetics and Biodistribution, and Reduce Immunogenicity. *Br. J. Cancer.* **1998**, *78*, 189–197.
39. Caliceti, P.; Chinol, M.; Roldo, M.; Veronese, F. M.; Semenzato, A.; Salmaso, S.; Paganelli, G. Poly(ethylene glycol)-Avidin Bioconjugates: Suitable Candidates for Tumor Pretargeting. *J. Controlled Release* **2002**, *83*, 97–108.
40. Salmaso, S.; Semenzato, A.; Bersania, S.; Chinol, M.; Paganelli, G.; Caliceti, P. Preparation and Characterization of Active Site Protected Poly(ethylene glycol)-Avidin Bioconjugates. *Biochim. Biophys. Acta* **2005**, *1726*, 57–66.
41. Moghimi, S. M.; Szebeni, J. Stealth Liposomes and Long Circulating Nanoparticles: Critical Issues in Pharmacokinetics, Opsonization and Protein-Binding Properties. *Prog. Lipid Res.* **2003**, *42*, 463–478.
42. Cattel, L.; Ceruti, M.; Dosio, F. From Conventional to Stealth Liposomes: A New Frontier in Cancer Chemotherapy. *J. Chemother.* **2004**, *16* (Suppl. 4), 94–97.
43. Livnah, O.; Bayer, E. A.; Wilchek, M.; Sussman, J. L. Three-Dimensional Structures of Avidin and the Avidin-Biotin Complex. *Proc. Natl. Acad. Sci. U.S.A.* **1993**, *90*, 5076–5080.
44. Jeon, S. I.; Andrade, J. D. Protein Surface Interactions in the Presence of Polyethylene Oxide 0.2. Effect of Protein Size. *J. Colloid Interface Sci.* **1991**, *142*, 159–166.
45. Jeon, S. I.; Lee, J. H.; Andrade, J. D.; Degennes, P. G. Protein Surface Interactions in the Presence of Polyethylene Oxide 0.1. Simplified Theory. *J. Colloid Interface Sci.* **1991**, *142*, 149–158.
46. Sofia, S. J.; Premnath, V.; Merrill, E. W. Poly(ethylene oxide) Grafted to Silicon Surfaces: Grafting Density and Protein Adsorption. *Macromolecules* **1998**, *31*, 5059–5070.
47. Wilbur, D. S.; Chyan, M. K.; Pathare, P. M.; Hamlin, D. K.; Frownfelter, M. B.; Kegley, B. B. Biotin Reagents for Antibody Pretargeting. 4. Selection of Biotin Conjugates for *in Vivo* Application Based on Their Dissociation Rate from Avidin and Streptavidin. *Bioconjugate Chem.* **2000**, *11*, 569–583.
48. Wilbur, D. S.; Hamlin, D. K.; Chyan, M. K.; Kegley, B. B.; Pathare, P. M. Biotin Reagents for Antibody Pretargeting. 5. Additional Studies of Biotin Conjugate Design to Provide Biotinidase Stability. *Bioconjugate Chem.* **2001**, *12*, 616–623.
49. Morpurgo, M. Investigation over the Affinity between Avidin and the Nucleic Acids. Manuscript in preparation, **2013**.
50. Lazzari, S.; Moscatelli, D.; Codari, F.; Salmona, M.; Morbidelli, M.; Diomede, L. Colloidal Stability of Polymeric Nanoparticles in Biological Fluids. *J. Nanopart. Res.*, *14*, 920.
51. Frangioni, J. V. *In Vivo* near-Infrared Fluorescence Imaging. *Curr. Opin. Chem. Biol.* **2003**, *7*, 626–634.
52. Ferrucci, J. T.; Stark, D. D. Iron-Oxide Enhanced MR-Imaging of the Liver and Spleen—Review of the first-5 Years. *Am. J. Roentgenol.* **1990**, *155*, 943–950.
53. Patel, V.; Papineni, R. V. L; Gupta, S.; Stoyanova, R.; Ahmed, M. M. A Realistic Utilization of Nanotechnology in Molecular Imaging and Targeted Radiotherapy of Solid Tumors. *Radiat. Res.* **2012**, *177*, 483–495.
54. Hiller, Y.; Gershoni, J. M.; Bayer, E. A.; Wilchek, M. Biotin Binding to Avidin -Oligosaccharide Side-Chain Not Required for Ligand Association. *Biochem. J.* **1987**, *248*, 167–171.
55. Achour, O.; Bridiau, N.; Kacem, M.; Delatouche, R.; Bordenave-Juchereau, S.; Sannier, F.; Thiery, V.; Piot, J. M.; Maugard, T.; Arnaudin, I. Cathepsin D Activity and Selectivity in the Acidic Conditions of a Tumor Microenvironment: Utilization in the Development of a Novel Cathepsin D Substrate for Simultaneous Cancer Diagnosis and Therapy. *Biochimie* **2013**, *95*, 2010–2017.
56. Blencowe, C. A.; Russell, A. T.; Greco, F.; Hayes, W.; Thornthwaite, D. W. Self-Immolative Linkers in Polymeric Delivery Systems. *Polym. Chem.* **2011**, *2*, 773–790.
57. Hao, T. N.; Qiao, M. X.; Li, Z.; Chen, D. W. Progress in the Study of Ph and Temperature Sensitive Biodegradable Block Copolymers. *Yaoxue Xuebao* **2008**, *43*, 123–127.
58. Peterson, J. J.; Meares, C. F. Cathepsin Substrates as Cleavable Peptide Linkers in Bioconjugates, Selected from a Fluorescence Quench Combinatorial Library. *Bioconjugate Chem.* **1998**, *9*, 618–626.